The discharge characteristics of motor units innervating functionally paralyzed muscles

american physiological society

JNP JOURNAL OF NEUROPHYSIOLOGY

J Neurophysiol 133: 343–357, 2025.
First published December 20, 2024; doi:10.1152/jn.00389.2024

RESEARCH ARTICLE

Neuroscience of Disease

The discharge characteristics of motor units innervating functionally paralyzed muscles

Daniela Souza De Oliveira,[1] Marco Carbonaro,[2] Brent James Raiteri,[3] Alberto Botter,[2] Matthias Ponfick,[4] and Alessandro Del Vecchio[1]

[1]*Department Artificial Intelligence in Biomedical Engineering, Friedrich-Alexander-Universität Erlangen-Nürnberg, Erlangen, Germany;* [2]*Laboratory for Engineering of the Neuromuscular System (LISiN), Department of Electronics and Telecommunication, Politecnico di Torino, Turin, Italy;* [3]*Human Movement Science, Faculty of Sport Science, Ruhr University Bochum, Bochum, Germany; and* [4]*Querschnittzentrum Rummelsberg, Krankenhaus Rummelsberg GmbH, Schwarzenbruck, Germany*

Abstract

For individuals with motor complete spinal cord injury (SCI), previous works have shown that spared motor neurons below the injury level can still be voluntarily controlled. In this study, we investigated the behavior of these neurons after SCI by analyzing neural and spatial properties of individual motor units using high-density surface electromyography (HDsEMG) and ultrasound imaging. The dataset for this study is based on motor unit data from our previous work (Oliveira et al. *Brain* 147: 3583–3595, 2024). Eight participants with chronic motor complete SCI and twelve uninjured controls attempted multiple hand movements, guided by a virtual hand, while we recorded forearm muscle activity. We analyzed the common synaptic input to motor neurons with a factorization method and found two dominant motor unit modes in both the SCI and control groups. Each mode was strongly correlated with the virtual hand's flexion or extension movements. The delay between flexion and extension movements and the motor unit modes was similar between groups, suggesting preserved common input to motor neurons after SCI. We classified motor units into task-modulated or nonmodulated (i.e., tonic or irregularly firing) based on their discharge patterns and phase difference with virtual hand kinematics and found a higher proportion of nonmodulated motor units in the SCI group. At the motor unit action potential level, we found larger motor unit territories after SCI. Finally, we observed distinct movements of paralyzed muscles with concurrent HDsEMG and ultrasound imaging, indicating the presence of highly functional motor units with distinct spared territories after SCI.

NEW & NOTEWORTHY Here, we observed a similar pattern of motor unit activation during attempted hand movements in individuals with complete SCI, who cannot move their fingers, and in a control group, who performed the prescribed movements. Despite differences in individual motor unit behavior between these groups, such as a higher proportion of nonmodulated motor units in SCI, movement intention can still be decoded from paralyzed muscles.

high-density surface electromyography; motor neuron; motor unit; spinal cord injury

INTRODUCTION

Following a spinal cord injury (SCI), a cascade of events occurs leading to the loss of synapses in spinal motor neurons (1), muscle fiber denervation (2), and motor neuron degeneration (3, 4). All of these events cause substantial changes to the afferent inputs and efferent outputs of spinal motor neurons (5). There has been evidence of corticospinal and spinal circuitry adaptation, with changes in synaptic strength and the formation of new cortical, subcortical, or spinal circuits (2, 6–8).

However, the mechanisms the nervous system uses to compensate for the damage from the injury are not well understood. Corticospinal reorganization can result as a function of natural recovery but can also result in maladaptation, and lead to spasticity, impaired muscle control, or the deterioration of other

Correspondence: A. Del Vecchio (alessandro.del.vecchio@fau.de).
Submitted 29 August 2024 / Revised 11 December 2024 / Accepted 12 December 2024

neural functions (3, 4, 6, 9, 10). Due to the diversity of injuries, intervention time, and subject-specific factors, individuals recover differently, even when the injuries have similar levels and classifications (11–13). Also, the loss of muscle function can vary according to the distance between motor neuron pools and the lesion site (14). Although animal models clarify some of these adaptation mechanisms (1, 15), there are still insufficient motor unit studies in humans to understand how motor unit properties are altered after SCI (16–19). This is because the type of injuries induced in animals (transection, contusion, compression) and the restrictions imposed by a laboratory environment can affect their recovery (5).

Recent (20–22) and past evidence (23–26) in humans suggest that some spinal motor neurons below the level of the SCI are still functional and that they can be voluntarily controlled, even when no voluntary movement can be observed. Despite the first evidence of residual muscle activity after complete SCI appearing over four decades ago (26), not much is known about neural or spatial properties of the spared motor units after SCI. Therefore, it is relevant to understand whether these neurons adapt after the injury and which properties make them functional. Few studies have used surface and intramuscular electromyography (16–19, 21), but many aspects have not been investigated in the spared motor unit population. Particularly, very little is known about how these motor units are modulated during controlled dynamic tasks and the peripheral rearrangements of motor units that may be detected with electromyography.

We aimed to use high-density surface electromyography (HDsEMG) and blind source separation to directly investigate the properties of spared spinal motor neurons in individuals with chronic motor complete SCI while they attempted fine hand movements. We applied the same techniques to a control group of uninjured individuals, performing the same tasks to understand possible motor neuron differences in individuals with and without SCI. The data included in this work are derived from our previous study (22). In the present work, we focused on the analysis of neural and peripheral motor unit properties of the SCI group and the comparison with the control group. The analysis of motor unit activity allows us to have a direct representation of the potential rearrangements of the neural output from the spinal cord and might provide insights into underlying recovery mechanisms. We extracted the patterns of activation of the spared motor neuron pools, common synaptic inputs, and motor unit territories within multiple forearm muscles. Moreover, we associated motor unit activity with localized muscle displacements in the forearm cross-section through concurrent recordings of HDsEMG and ultrasound in two participants with SCI.

We found clear patterns of motor unit activity with distinct muscular territories that encoded specific movements of the hand. In addition, we found that these motor neuron activation patterns were similar between the groups, even though there were clearly fewer task-modulated motor units after SCI. This suggests that highly functional common inputs are preserved after SCI and that control algorithms can benefit from the identification of the modulated motor units to develop high-performance brain-machine interface systems for assistive devices.

MATERIALS AND METHODS

Participants and Ethical Approval

In this study, eight participants (3 women) with chronic cervical spinal cord injury were recruited in the SCI group. The inclusion criteria were ages between 18 and 60 yr, chronic injury (>1 year), absence of voluntary movement in one or both hands and an SCI level between C4 and C6. Table 1 describes the data set and participants' characteristics. In addition, 12 young uninjured adults (2 women) were recruited in the control group (age 27.1 ± 3.4 yr). Participants from both groups signed a written informed consent approved by the ethics committee of the Friedrich-Alexander-Universität Erlangen-Nürnberg, under the numbers 21-150B and 22-138Bm. The procedures were in agreement with the Declaration of Helsinki, except for database registration.

Experimental Protocol

The results presented in this study were collected during one main laboratory visit. During this visit, we placed four or five electrode grids over the forearm muscles of the participants' dominant arm. After that, prerecorded videos of a moving virtual hand were shown to the participants, and eight tasks were attempted by them. Five tasks included extension and flexion of each finger (thumb, index, middle, ring, and pinkie finger), and the three other tasks were opening and closing of the fingers, and two- and three-finger pinches with a movement frequency of 0.5 Hz (2 s period, total duration of 42 s). Periodic tasks were chosen to investigate patterned motor unit activity and assess whether motor units can sustain this pattern over time. The participants were instructed to attempt the task shown on the monitor in front of them and follow the movement in the video as best as they could. We recorded each participant's muscle activity while they attempted each task. The familiarization period with the tasks was not different between groups and lasted 5–10 s per task. The virtual hand videos (8 tasks, 0.5 Hz, 42 s duration each) were based on a 3-D virtual hand model generated with Blender software (Blender 3.0, Blender Foundation).

SCI Group

Four or five electrode grids (64 electrodes per grid, in total either 256 or 320 electrodes) were placed over the forearm muscles of the participants. Whether four of five grids were used depended on the participant's arm circumference. The participants sat in a comfortable position in their own wheelchairs and performed each task 1–2 times. If the task was performed more than once, then the recording with more decomposed motor units was subsequently analyzed. It is important to note that the participants of the SCI group were not executing the movements, but only attempting the tasks, as they are not able to move their fingers (Supplemental Video S1).

Control Group

We placed five electrode grids (320 electrodes) over the forearm muscles of all participants of this group. The participants were then instructed to perform the same hand tasks with the same frequency and duration as in the SCI group

Table 1. *Description of research participants, injury details, and average number of MUs identified per task, means (SD) for each participant*

Participant	Age (Years)	Gender	Injury Level	AIS	Wristmovement	Time since Injury (Years)	Sensory Level[a]	Spasticity upper limb (MAS)[b]	Stretch Reflexes upper limb	Note	MUs/Task
S1	39	M	C6	B	Yes	18.8	S5	0	Absent	Tenodesis	14.5 (2)
S2	34	M	C5	B	Yes	9.1	C5	0	B: reduced; BR, T: absent	Tenodesis	8.1 (1.2)
S3	41	F	C6	B	Yes	24.2	C6	0	B, BR: exaggerated; T: absent	Tenodesis	3.5 (1.4)
S4	39	F	C5	A	Yes	24.2	C5	0	Normal		7.3 (2.3)
S5	34	M	C6	A	No	22.2	C6	0	Absent		8.4 (0.7)
S6	57	M	C5	A	No	6.9	T3	Right: 2, Left: 0	Right: reduced; Left: exaggerated	Botox right arm	22.8 (4.2)
S7	44	M	C6	C	No	18.2	C6	Right: 2, Left: 0	Right: exaggerated; Left: reduced		7.4 (2)
S8	38	F	C5	B	Yes	5.0	T1	1	Absent		5.9 (1.2)

AIS, ASIA Impairment Scale; B, biceps reflex; BR, brachioradialis reflex; MAS, Modified Ashworth Scale; MU, motor units; T, triceps reflex. [a]Sensory level corresponds to the lowest level with normal sensory function. [b]Spasticity was assessed for elbow flexion.

according to the virtual hand videos. Most tasks were performed once in this group. The kinematics of the hand were also captured with a set of cameras (model DFK-37BUX287, The Imaging Source, Bremen, Germany), which was not possible in the SCI group due to complete hand paralysis. The setup was similar to the one already described in [Cakici et al., (27)]. The participants were standing with their hands inside a framework with the camera setup.

HDsEMG Recordings

We recorded the HDsEMG signals in monopolar mode with a multichannel amplifier, 16-bit A/D, bandpass filter of 10–500 Hz, and sampling frequency of 2,048 Hz (Quattrocento, OT Bioelettronica, Turin, Italy). Before applying the electrode grids, we shaved the forearm skin of the participants and cleaned it with 70% ethyl alcohol. The electrode grids were placed on the surface of the forearm over the skin, with two or three grids around the forearm aligned to the ulna bone [8 rows $\times$ 8 columns, interelectrode distance (IED) 10 mm, OT Bioelettronica, Turin, Italy] and two grids around the wrist, above the wrist joint (13 $\times$ 5, IED = 8 mm). We attached the electrode grids to the skin using bi-adhesive foam, conductive paste (SpesMedica, Battipaglia, Italy), and tape. The ground electrode was dampened with water and placed over the styloid process of the ulna, and the reference electrode was placed on the elbow joint, over the olecranon. We used a trigger signal from a microcontroller to start the virtual hand videos and later used this signal to synchronize the EMG recordings with the videos.

Combined HDsEMG and Muscle Ultrasound Recordings

In a second session, we simultaneously recorded HDsEMG signals and B-mode ultrasonography from the forearm cross-section of participants S2 and S4 from the SCI group. The participants performed the same tasks as in the first session, as well as a wrist movement since these participants could move their wrists. Concurrently, an ultrasound transducer was handheld in the transverse plane either on top of a transparent HDsEMG grid (S4) (28) or next to a HDsEMG grid (S2) over the forearm extensor muscles. For the measures of S4, we used a system of electrodes transparent to ultrasound (8 $\times$ 4 electrodes, IED = 10 mm in both directions). This system enables simultaneous recordings of HDsEMG and ultrasonography from the same muscle region and has been used to study neuromechanical muscle properties, both at the global level and single motor unit level (29, 30). The grid of electrodes was aligned to the ulna bone, similar to previous recordings, and the ultrasound transducer was placed on the top of the grid to obtain cross-sectional images of the forearm extensor muscles (Fig. 3*A*). Ultrasound images were captured using B-mode ultrasonography with a flat linear-array transducer (6 MHz, ~170 frames/s, 60 mm field of view; LV8-5N60-A2, Telemed, Vilnius, Lithuania) controlled by the PC-based ArtUs EXT-1H scanner (Telemed). HDsEMG signals were recorded with a wireless wearable amplifier (MEACS - LISiN, Politecnico di Torino and ReC Bioengineering Laboratories, Torino) (31). A synchronization pulse generated by the ultrasound system at the start of the acquisition was recorded by the HDsEMG system to synchronize the recordings. The monopolar HDsEMG signals were decomposed into individual motor unit spike trains with the approach described in the next subsection.

HDsEMG Decomposition

First, the monopolar HDsEMG signals were bandpass filtered (20-500Hz) with a second-order Butterworth filter and a 50 Hz notch filter was applied. We rearranged the signals from all electrode grids into a single matrix (13 rows $\times$ 26 columns, Fig. 5*A*). To decompose the HDsEMG signals into individual motor units, we applied a convolutive blind source separation algorithm through the DEMUSE software (v. 4.5; The University of Maribor, Slovenia) (32), which automatically identified the motor unit spike trains of multiple motor units. We directly removed motor units with a pulse-to-noise ratio $<$ 26 dB and after visual inspection and manual editing of the motor unit spike trains, we kept motor units with a pulse-to-noise ratio $\geq$ 30 dB only as described in the study by Del Vecchio et al. (33).

Data Analysis

Common drive and latent factor analysis.

For each of the eight tasks performed, we applied a nonnegative matrix factorization (NNMF) method to the detrended smoothed motor unit spike trains (1 s Hanning window, considering the period of our tasks) of all decomposed motor units (34, 35), except when the number of motor units was less than two. We used the *NNMF* function in MATLAB (R2022b, The MathWorks, Inc, Natick, MA) and allowed 1,000 iterations and a constraint of five factors/modes. This method is a dimensionality reduction technique used to extract underlying features of a data set and was applied due to its ability to extract interpretable, nonnegative components. This function thus estimated the common motor unit modes associated with the observed data, i.e., the filtered motor unit spike times (36). As NNMF identified two motor unit modes that explained most of the data variance, we performed a cross-correlation between each factor/mode and the resampled reference kinematics according to the signal sampling rate (2,048 Hz). The reference kinematics corresponded to the movement of the virtual hand. We performed this cross-correlation step to test whether differences in the common drive between the SCI and control groups existed, and if the modes corresponded to flexion or extension of the individual fingers based on their similarity to the reference kinematics. We obtained the cross-correlation value and time delay between the signals (i.e., lag) for each of the eight tasks. We limited the lag to a maximum of 2 s, which was the period of the reference kinematics. We assumed that our data would be explained by a linear combination of the common factors associated with most of the data variance. We calculated the percentage of the total variance explained by these factors for each task from each participant and later averaged this variance across all tasks for one participant.

Motor unit classification based on NNMF.

The NNMF approximates the motor unit data set for each task as $V \approx WH$, where W contains the motor unit modes, and H contains the weight coefficients representing the contribution of each motor unit to these modes, with values from 0–1. Since we considered two modes, each motor unit is associated with two weight coefficients, one related to the extension mode (ext coefficient) and the other to the flexion mode (flex coefficient). To classify motor units according to their association with these modes, we sorted the values of the H-matrix for each task, based on the cross-correlation between each mode and the reference kinematics described in the previous subsection. A classification threshold was defined by observation as $H_i > 2H_j$ and $H_i > 0.25$, where H_i and H_j can represent either ext or flex coefficients. Depending on the weight coefficients, motor units were associated with one (flexion or extension) or two modes (referred to as nonmodulated).

Phase analysis.

Given that we successfully extracted two modes for each task using NNMF, we decided to investigate the behavior of the motor units in each task. For that, we assessed the phase difference between the smoothed spike trains of each individual motor unit (1 s Hanning window) and the reference kinematics. We used this phase difference to compare the performance of each group in following the reference kinematics. We chose a period of 18–40 s for this comparison after considering the familiarization time with the tasks. First, we applied a Hilbert transform to convert the signals (reference kinematics and smoothed motor unit spike trains) into complex numbers and extracted their amplitude and phase angles. We then computed the phase difference by subtracting the reference kinematics phase angles from the motor unit phase angles, generating a phase histogram for each motor unit.

To understand if the behavior of the motor units was task-modulated (i.e., associated with flexion or extension movements) or nonmodulated, we computed the circular variance of the phase difference histogram, which has a scale from 0–1. Circular variance is used here as a measure of phase difference consistency and is mathematically equivalent to the inverse of the phase-locking value (i.e., 1 – phase-locking value). A low variance (i.e., low dispersion of the data) indicates that the phase difference angles point mainly in the same direction, with a consistent phase delay. A high variance value indicates that the phase difference angles are very spread (multidirectional). While the variance does not necessarily separate modulated and tonic motor units, it indicates if a motor unit is firing with a consistent phase difference throughout the recording. To quantify the proportion of motor units consistently aligned with the reference kinematics and those with more variable firing patterns, we classified all motor units of each participant into task-modulated (low variance, var $<$ 0.3) and nonmodulated (high variance, var $>$ 0.7). We then computed the percentage of modulated and nonmodulated motor units for each participant. The variance threshold was defined to account for differences between the groups based on the variance of the phase difference histograms (Fig. 2*B*). We also calculated the total number of modulated and nonmodulated motor units for both groups.

In addition, we calculated the circular kurtosis of the phase difference distributions to assess their tailedness, which indicates whether the distributions' tails are light or heavy. This analysis was included to verify if the results from circular variance were consistent with the kurtosis, as the variance does not provide information about the shape of the phase difference distribution. A low kurtosis indicates a more uniform and flatter distribution, while a high kurtosis value suggests a sharper peak around the mean phase difference, possibly reflecting a more consistent firing pattern of motor units. The kurtosis was calculated using a circular statistics toolbox for MATLAB (37).

Estimation of muscle tissue displacement with ultrasound.

Ultrasound videos were processed in MATLAB to detect muscle tissue displacement. The velocity of the muscle tissue displacement was estimated by computing the optical flow using the Horn-Schunck method, which is a global differential technique (38). This method required a smoothing parameter, which was set to 1 because limited displacement was expected in the cross-sectional images of the forearm extensor muscles, and a parameter of maximum iterations set to 10, which is a default value to estimate the optical flow of objects with relative medium-low velocity. This procedure provides the magnitude of the tissue velocity for each pixel of each image. Each image was then filtered with a 2-D Gaussian smoothing kernel with sigma equal to 20 to reduce the speckle noise and to obtain a smoother spatiotemporal representation of the muscle tissue displacement.

To obtain a spatial and temporal representation of the muscle motion, singular value decomposition was applied to the image sequence. The first principal component was retained and transformed into one *eigen-image* (hereafter referred to as the *tissue displacement image*), which identified the muscle region where the primary displacement occurred, and one *eigen-time course* (hereafter referred to as the *tissue displacement time course*), which described how the tissue displacement image evolved over time.

Analysis of combined HDsEMG and ultrasound recordings.

The spatial agreement between tissue displacement regions and EMG amplitude distributions was assessed for both global [root-mean-square (RMS) maps] and single motor unit signals. Moreover, the correlation between the temporal evolution of tissue displacement and the neural input to the muscle was performed. The following procedure was adopted: *1*) individual motor units spike trains were summed to generate a cumulative spike train (CST); *2*) the CST was convoluted with a 1 s Hanning window; *3*) the convoluted CST and the tissue displacement time course were lowpass filtered (4th-order zero-phase Butterworth, 2 Hz) and then high-pass filtered (4th-order zero-phase Butterworth, 0.75 Hz); *4*) the cross-correlation between these filtered signals was computed in 5-s segments with 50% overlap (30). Finally, the average cross-correlation coefficient and the delay were computed across segments.

Spike-triggered average and motor unit amplitude.

We applied a notch filter at 50 Hz and a bandpass Butterworth filter (second-order, zero lag, 20 and 500 Hz cut-off frequencies) to the monopolar HDsEMG signals as a preprocessing step. We discarded data from electrodes that deviated by more than three standard deviations (SD) from the average RMS values (μV) across all electrodes. Through the spike times obtained after the decomposition process, we obtained the motor unit action potential waveforms from the preprocessed HDsEMG signal by applying the spike-triggered average method. A centered 100-ms window was used on each spike time and averaged across all spike times of the respective motor unit, for each electrode. After that, we calculated the peak-to-peak amplitude of the motor unit action potentials, identified the three highest peak-to-peak values, and calculated their average for each motor unit in each task. We analyzed the motor unit amplitude because it can be representative of reinnervation (16).

Motor unit spatial properties.

Based on the RMS values of the motor unit action potentials, a spatial map was created to represent the amplitude distribution of each motor unit. Therefore, the individual grids from each task recording were combined to match the grid placement on the forearm (Fig. 5). Using the image processing toolbox of MATLAB, we normalized the scale of each map (from 0 to 1, where 1 indicates maximum activity) and calculated the motor units' total area of activity. We summed the number of pixels with intensity values higher than a threshold of 0.7 and multiplied it by the electrode area, area = 64 mm^2 (IED = 8 mm) or area = 100 mm^2 (IED = 10 mm). We obtained the total area by considering in which electrode grid the motor unit activity was identified.

To evaluate each identified motor unit's size and relative depth, we decided to correlate its maximum peak-to-peak amplitude and area. This is because peak-to-peak amplitude alone is not an adequate estimator of motor unit size (39).

Reconstructed EMG signals.

We wanted to investigate if any differences in area and amplitude values between the groups could be explained by their amount of undecomposed motor units. Therefore, we reconstructed the EMG signals to compare the number of active motor units we could decompose in both SCI and control groups. The sum of the motor unit action potential shapes obtained with the spike-triggered average was convolved with the motor unit firings to reconstruct the EMG signal. We used the root mean square error (RMSE) between the original (O) and reconstructed EMG signals (R) to indicate the relative amount of undecomposed motor units.

We calculated the RMSE for the individual electrodes, with N as the number of samples, and for each task, we averaged these values across all electrodes:

$$\mathrm{RMSE} = \sqrt{\frac{\sum_{i=1}^{N}(R_i - O_i)^2}{N}}.$$

Statistical Analysis

Due to our small number of participants and the possibility of outliers biasing the mean, we opted for a nonparametric approach. The results are presented as median [interquartile range (IQR)] when the data did not follow a normal distribution. To assess the statistical differences between the groups, we used a generalized linear mixed-effects model (*glmer*, MATLAB) according to the equation: variable of interest ~ task × group + (1 | participant), group and tasks were considered as fixed-effects, and the participants as a random effect. For the explained variance comparison across five modes, we used the equation: explained_variance ~ mode × group + (1 | participant). For the variables phase difference variance, kurtosis, and motor unit spatial distribution, we used only: variable of interest ~ group + (1 | participant). Based on the variable of interest and considering the model with the lowest Akaike Information Criterion (AIC), we chose an appropriate data distribution (normal, inverse Gaussian, or gamma). For

coefficient estimation, we used the maximum pseudo-likelihood (MPL) or Laplace methods, also according to the model with the lowest AIC. We reported the group estimate (β), *t* statistic (degrees of freedom) – *t*(df), and *P* value (significance level or α value < 0.05). This approach accounts for the non-normality of the data and the differences in number of motor units across tasks, participants, and groups.

To analyze the differences in the number of modulated and nonmodulated motor units between SCI and control groups, we applied Welch's *t* test (unequal variances). For the correlation between kurtosis and variance of phase difference, as well as area and peak-to-peak amplitude, we chose Spearman correlation, as we expected a nonlinear, but monotonic relationship between these variables.

RESULTS

In this study, we compared motor unit neural and spatial properties between two groups [SCI: $n = 8$, age 40.7 yr (SD = 7.3); control: $n = 12$, age 27.1 yr (3.4)]. Moreover, we analyzed the motor unit discharge patterns across all attempted movements of the SCI group to directly demonstrate the amount of common synaptic inputs received by the population of motor units. Figure 1*A* shows an overview of the experimental setup. In total, 622 motor units were identified in the SCI group [9.72 (6.11) motor units per task/participant] and 766 in the control group [7.98 (4.08) motor units per task/participant]. We found no significant difference in the number of detected motor units between groups [$P = 0.27$, $t(144) = 1.10$, $\beta = 0.007$]. A detailed description of the SCI data set can be

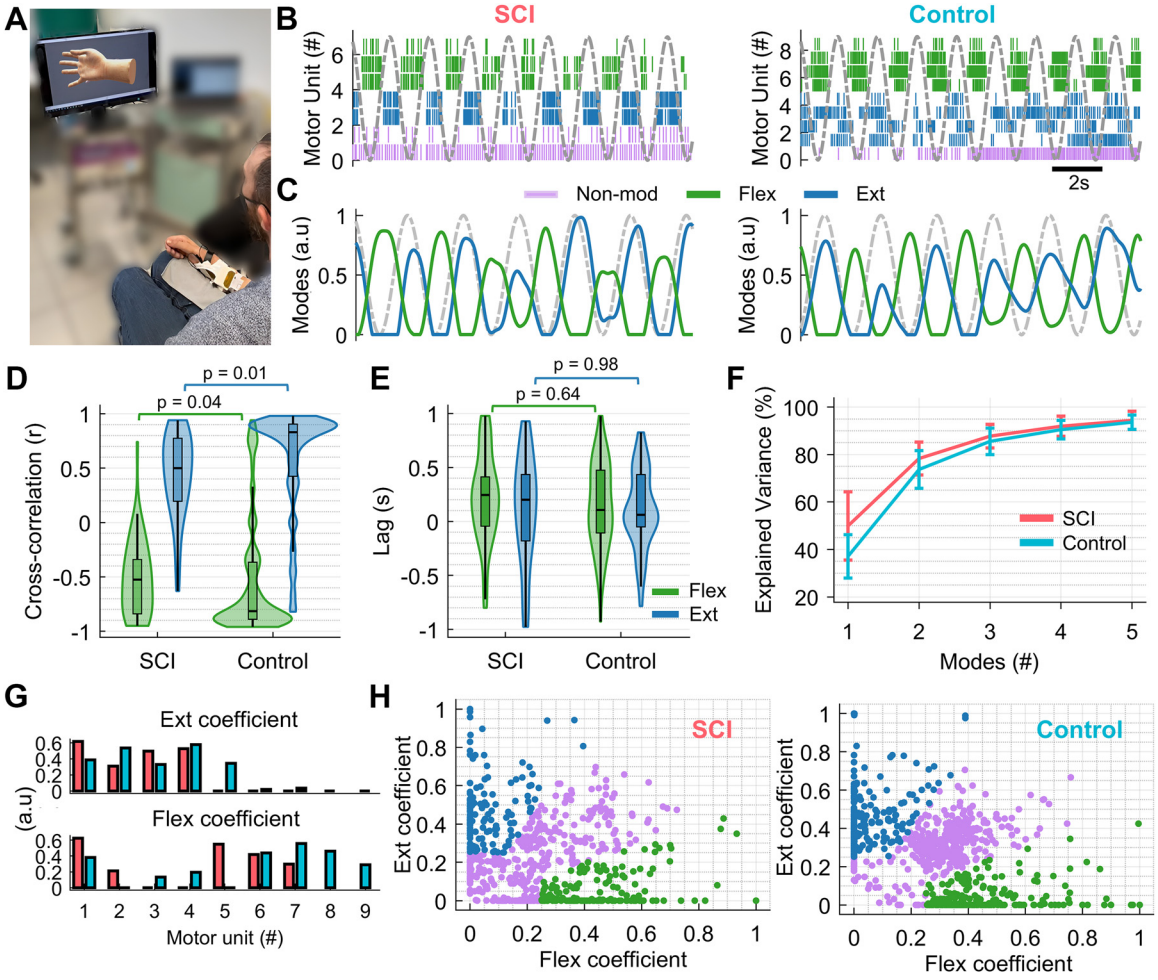

Figure 1. *A*: one participant from the spinal cord injury (SCI) group following virtual hand video instructions with grids of electrodes over their forearm. Note that the participants in the SCI group were only attempting the movements, as they were unable to move their fingers. *B*: on the left and right, motor unit firings identified during the ring finger task from participant S4 and participant C10 are shown, respectively. Examples of motor units encoding flexion (flex, in green), extension (ext, in blue), or nonmodulated motor units (nonmod, in purple) are shown. The dashed grey curve corresponds to the reference kinematics of the virtual hand. *C*: two main motor unit modes were extracted with nonnegative matrix factorization (NNMF) from the tasks in *B*, flex (in green), and ext (in blue). The reference kinematics are shown in dashed gray. *D*: cross-correlation results between reference kinematics and the motor unit modes extracted for each task (8 tasks per participant). The modes were distinguished according to positive (ext) and negative (flex) cross-correlation, or ext > flex values in cases where both values were positive or negative. *E*: lag values between each motor unit mode and the reference kinematics. The maximum lag was limited to the period of the movement (2 s). *F*: explained variance for both groups according to the number of modes extracted. The variance was averaged across tasks and participants for SCI (pink) and control (blue) groups. *G*: example of weight coefficients obtained from the NNMF results for the motor units shown in *B*, SCI (pink) and control (blue). Each motor unit is associated with two values, ext and flex coefficients, representing the motor unit's contribution to each mode. *H*: classification of motor units based on the weight coefficients for both the SCI and control groups. Motor units are color-coded according to their classification as flexion, extension, or nonmodulated, as shown in *A*.

found in Table 1, which was first presented in our previous publication (22).

Motor Unit Modes during the Attempted Hand Movements

Based on the smoothed motor unit spike trains, we obtained two main motor unit modes (i.e., the latent factors extracted using the factorization algorithm) from each participant task (Fig. 1*C*). Only two modes explained nearly all the variance of the motor unit discharge characteristics and the kinematics of the virtual hand. Specifically, both motor unit modes closely matched the flexion and extension movements of the control virtual hand based on the cross-correlation between the kinematics of the virtual hand and the latent factors. The latent factors represent the combined activity of the smoothed discharge rates of motor units within each mode.

We associated each mode with the individual fingers' flexion (flex), or extension (ext) based on the cross-correlation sign, negative or positive, respectively. In the case of both negative or both positive values, we adopted ext > flex (e.g., ext = 0.9 and flex = 0.6; ext = −0.6, flex = −0.9). The positive and negative values were sorted according to the reference kinematics; extension was positively correlated with the reference, and flexion was negatively correlated with the reference. The activation of motor units during extension was aligned with the peaks in the reference kinematics, and motor unit activation during flexion was aligned with the troughs in the reference kinematics (Fig. 1*B*). Overall, our analysis revealed less similarity between the motor unit modes and the reference kinematics of the SCI group (Fig. 1*D*). This group showed lower cross-correlation values [median (IQR): flex = −0.53 (−0.84, −0.35); ext = 0.50 (0.21, 0.78)] in comparison with the control group [flex = −0.82 (−0.89, −0.42); ext = 0.84 (0.55,0.91)]. These results indicate that motor units in the control group were more correlated with the movements of the virtual hand in comparison to the SCI group. The distribution of cross-correlation values was significantly different between SCI and control groups [P_{flex} = 0.0391, $t(151) = -2.080$, $\beta = -0.337$; $P_{ext} = 0.0113$, $t(151) = 2.562$, $\beta = 0.412$]. Despite this difference, and considering that the SCI group was only attempting the tasks without being able to move their fingers, we found that both modes represented a distinct distribution of the motor unit discharge patterns encoding flexion and extension for both groups (Fig. 1, *B* and *C*).

In contrast, we observed no significant difference in lag values [SCI: flex = 253 ms (−50, 413); ext = 202 ms (−186, 438); control: flex = 116 ms (−115, 491); ext = 70 ms (−62, 443)] between SCI and control groups [$P_{flex} = 0.641$, $t(151) = 0.467$, $\beta = 65.757$; $P_{ext} = 0.971$, $t(151) = -0.0366$, $\beta = -5.5078$]. The lag values correspond to the time difference between the virtual hand kinematics (as displayed on the monitor) and the smoothed motor unit discharge patterns extracted by NNMF (Fig. 1*E*). These comparable lag values indicate that motor units were still being timely recruited after SCI to match the reference kinematics, which indicates a preserved common input to motor neurons.

The explained variance (Fig. 1*F*) was similar between groups when considering the two modes that explained most of the variance, 78.1% (SD = 9.5) and 74.0% (13.7) for SCI and control groups, respectively [$P_{mod\ =\ 2} = 0.211$, $t(153) = 1.256$, $\beta = 0.0745$]. For all five modes extracted, we found a significant difference between the groups [$P_{mod\ =\ 1\text{-}5} = 0.000508$, $t(721) = -3.492$, $\beta = -0.121$], with the first mode being the most discrepant [SCI: 49.4% (17.1); control: 37.4% (20.3)]. These results reveal that, despite the injury, the motor neurons detected in SCI still received common input, similar to the control group, and this motor unit activity was mainly controlled by two modes.

As we found mainly two motor unit modes associated with the active motor units, we attempted to classify the motor units based on these modes using the weight coefficients (ext and flex coefficients) extracted from the NNMF analysis (Fig. 1, *G* and *H*). We observed more motor units with low weight values (less than 0.25) in the SCI group. A greater number of motor units was classified as nonmodulated for both groups (SCI: 53.4%, control: 46.2% of the total of motor units), compared with task-modulated motor units for flexion (SCI: 20.8%, control: 26.2%) and extension (SCI: 25.8%, control: 27.5%).

Motor Unit Discharge Patterns during the Attempted Hand Movements

Since the classification based on NNMF approximates the motor unit data set, we then investigated the motor unit discharge characteristics at the individual motor unit level. By using the phase difference between the motor unit discharges and reference kinematics, and their variance values, we could identify motor units with a consistent phase difference (task-modulated) and varying phase (nonmodulated) during the analyzed section of the recording (Fig. 2*A*). Within the task-modulated motor units, we observed distinct patterns of activity characterizing flexion and extension motor units, including spatial differences (Fig. 2 *A*). We found a significant difference between the phase difference variance across groups [$P = 7.463\text{e-}10$, $t(1,386) = -6.20$, $\beta = -0.212$]. For SCI, most motor units presented a high phase difference variance, above 0.7, while the opposite was observed for the control group, in which many motor units had a phase difference variance below 0.3 (Fig. 2*B*). To verify whether the results of the phase difference variance were consistent, we analyzed the kurtosis (Fig. 2*C*). We observed a correlation between variance and kurtosis of phase difference for both groups [SCI: $r = -0.82$, $P < 0.0001$, control: $r = -0.95$, $P < 0.0001$). These results suggest that motor units with low phase difference variance are associated with high kurtosis, which indicates a peaked distribution. This association implies that the firing patterns of these motor units are more consistent and aligned with the reference kinematics. A histogram of the kurtosis values is also presented, showing that more motor units from the control group exhibited high kurtosis values, with a significant difference between SCI and control groups [$P = 1.006\text{e-}09$, $t(1,386) = 6.151$, $\beta = 0.182$].

Considering the phase difference variance (Fig. 2*D*), we observed a lower number of modulated motor units in the SCI group, though not statistically significant [SCI = 12.5 motor units/participant (8, 18); control = 28 motor units/participant (21.5, 35); Welch's *t* test, $t(10.61) = -1.667$, $P = 0.125$ two-tailed]. In contrast, the number of nonmodulated motor units was significantly higher for the SCI group [SCI = 28 motor units/participant (20.5, 39); control: 10 motor units/participant (6.5, 13.5); Welch's *t* test, $t(7.97) = 3.550$, P =

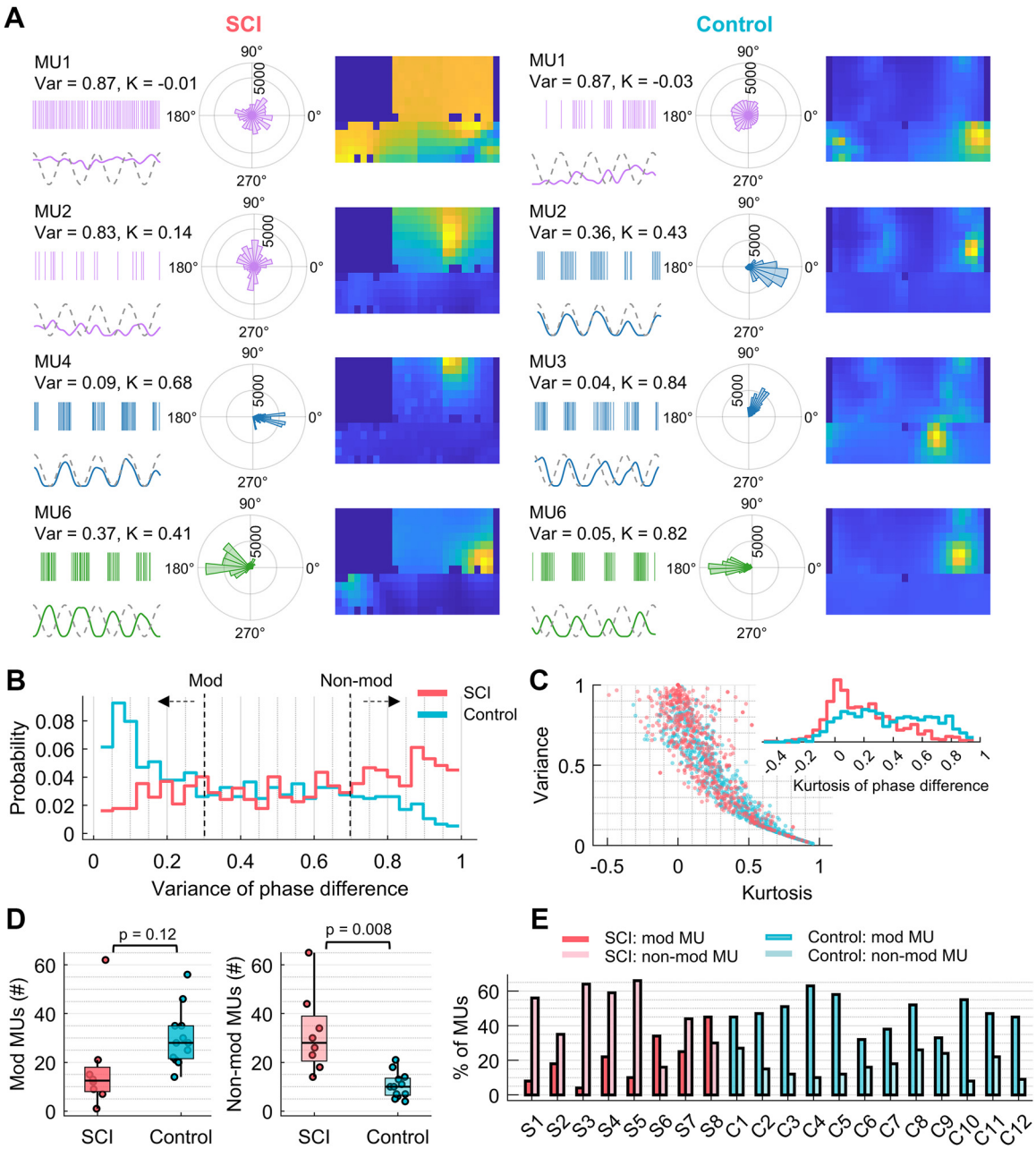

Figure 2. *A*: circular histograms representing the phase differences between the smoothed spike trains of a motor unit and the reference kinematics. Examples of flexion and extension-modulated motor units are shown in green and blue, respectively. Nonmodulated motor units that discharge irregularly are shown in purple. These motor unit examples are the same as presented in Fig. 1*B*. For each histogram, the spike trains of the corresponding motor unit and the smoothed spike trains compared with the reference kinematics are shown, along with the variance (var) and kurtosis of phase difference (K). The spatial map of motor unit action potential activity based on their root mean square (RMS) values is also displayed. *B*: histogram of the phase difference variance across all motor units from both groups, with spinal cord injury (SCI) in pink and control in blue. A phase variance near zero corresponds to modulated motor units (consistent phase, var $<$ 0.3), and a phase variance near one corresponds to nonmodulated motor units (var $>$ 0.7). Here, the contrast between the number of modulated units in both groups can be seen. *C*: correlation between variance and kurtosis of phase difference across all motor units for both groups. A kurtosis near zero or negative indicates a "flat" phase difference distribution, while a kurtosis near one represents a "peaked" distribution. This metric is correlated with the variance, complementing our analysis and showing that low variance is associated with high kurtosis. The histogram on the right displays the phase difference kurtosis across all motor units from both groups, with SCI in pink and control in blue. *D*: number of modulated (mod) and nonmodulated (nonmod) motor units per group based on the phase difference variance, with dots representing each participant. *E*: percentage of modulated (pink and blue, var $<$ 0.3) and nonmodulated motor units (light pink and light blue, var $>$ 0.7) for each participant. S6 and S8 are the only participants from the SCI group with more modulated units than nonmodulated ones, similar to the control group.

0.00755 two-tailed]. When observing the differences across participants in Fig. 2*E*, only S6 and S8 from the SCI group presented a higher ratio of modulated/nonmodulated motor units, similar to the control group.

Muscle Ultrasound Recordings

From the analysis of the ultrasound recordings, we identified different regions of displacement within the forearm muscles for different hand movements, according to the tissue displacement images. Figure 3*B* shows the results of three illustrative tasks of participant S4 wherein the tissue displacement region spatially agreed with the global RMS maps and the motor unit action potentials distribution of a representative motor unit. Figure 3*C* expands the middle finger movement example of Fig. 3*B* and shows that all three decomposed motor units locally corresponded with the ultrasound image displacement region. Figure 3*D* shows the fluctuations of the tissue displacement time course and the convoluted CST of the three decomposed motor units. Moderate cross-correlation between these signals (Fig. 3*E*) was observed (peak of mean cross-correlation = 0.4, delay = 118 ms), which indicates that the displacement of the muscle was in accordance with the firings of the motor units. It is worth noting that the tissue displacement time course in Fig. 3*D* refers to the magnitude of the velocity, and thus it depicts the phases of contraction (extension) and relaxation (flexion) of tissue with the same sign (both positive) despite being opposite directions.

Motor Unit Amplitude

The maximum peak-to-peak amplitudes of motor unit action potentials are shown in Fig. 4 across tasks, participants, and groups. Figure 4*B* shows that a few participants had higher amplitudes, S1 and S8, with the highest amplitude of 2724.4 μV from S1, in contrast to the control group, with the highest amplitude of 1778.3 μV from C9. Nonetheless, the amplitudes between groups did not differ significantly (Fig. 4*C*), and there was higher variability in the SCI group [SCI: 162.3 μV (108.8, 227.9); control: 151.9 μV (114.9, 187.6); $P = 0.456$, $t(1384) = 0.745$, $\beta = 16.06$].

Motor Unit Territory

The motor unit territory is represented by the area, indicating the spread of individual motor unit activity (Fig. 5*A*). We found, overall, a larger and more variable motor unit area in SCI compared with the control group [SCI = 560.0 mm^2 (405.7, 1082.5); control = 448.0 mm^2 (318.5, 564.9)]. These

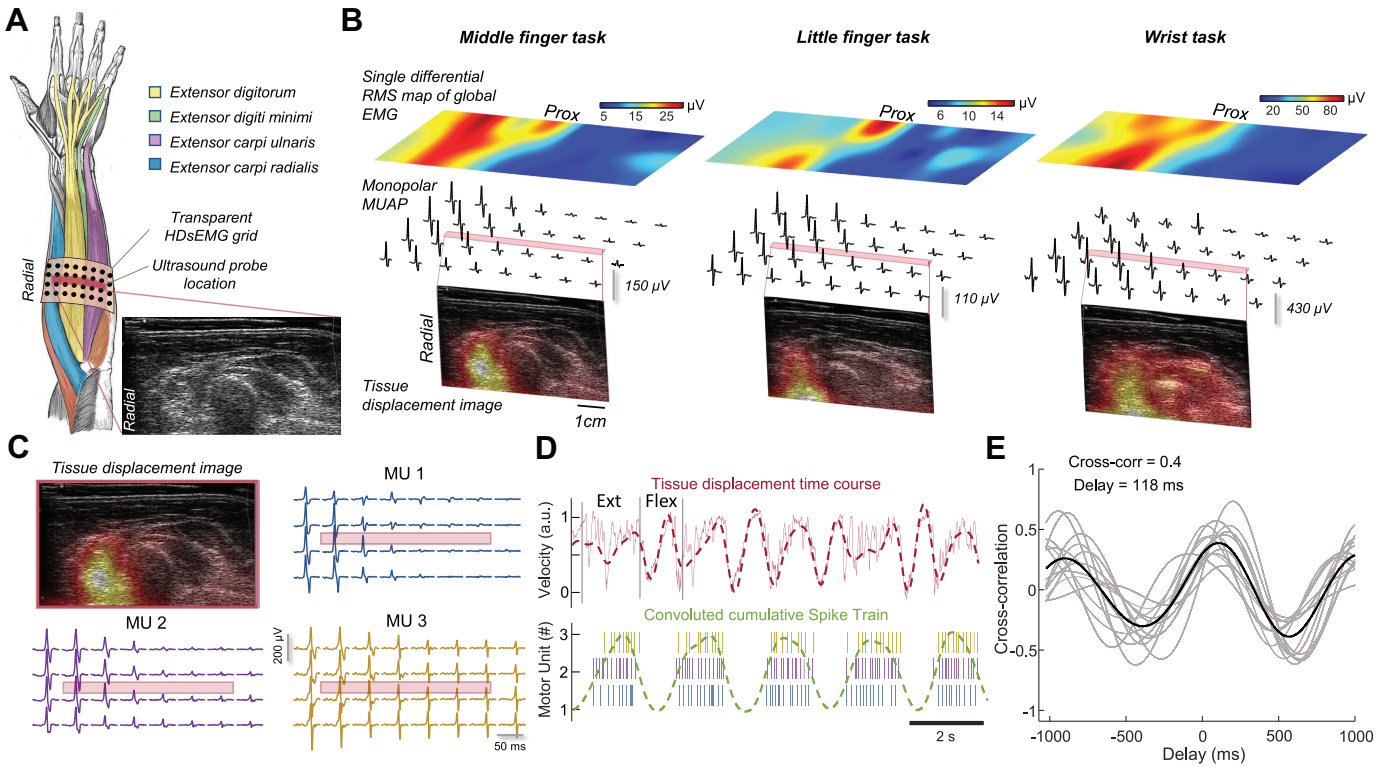

Figure 3. *A*: experimental setup showing the combined high-density surface electromyography (HDsEMG) and ultrasound measurements from the right forearm. The transducer was placed in the center of the ultrasound-transparent grid over the extensor muscles in the transverse plane. *B*: examples from three tasks (middle finger, little finger, and wrist flexion and extension) of the 3-D spatial agreement between the EMG signals and the principal tissue motion detected by B-mode ultrasound imaging. The *top panels* show the spatial activation maps determined from RMS values of single differential signals along the proximodistal direction. The *middle panels* show an example of the action potentials of decomposed motor units in monopolar derivation. In the *bottom panels*, the eigen-images of the first principal components (*tissue displacement image*) identified from the magnitude of the velocities computed from the ultrasound videos are overlapped on the B-mode images. *C*: eigen-image of the principal component and all three decomposed motor units of the middle finger task. The red transparent boxes show the location of the ultrasound transducer in the center of the grid. *D*: common fluctuations of the two generated signals of the middle finger task: ultrasound tissue displacement time course (red) and convoluted cumulative spike train of all three decomposed motor units (green). *E*: cross-correlation and lag (delay, ms) results between filtered signals of panel d. Gray lines represent the cross-correlation of 5-s overlapped segments (50% overlap) and the black line is the average cross-correlation of all segments.

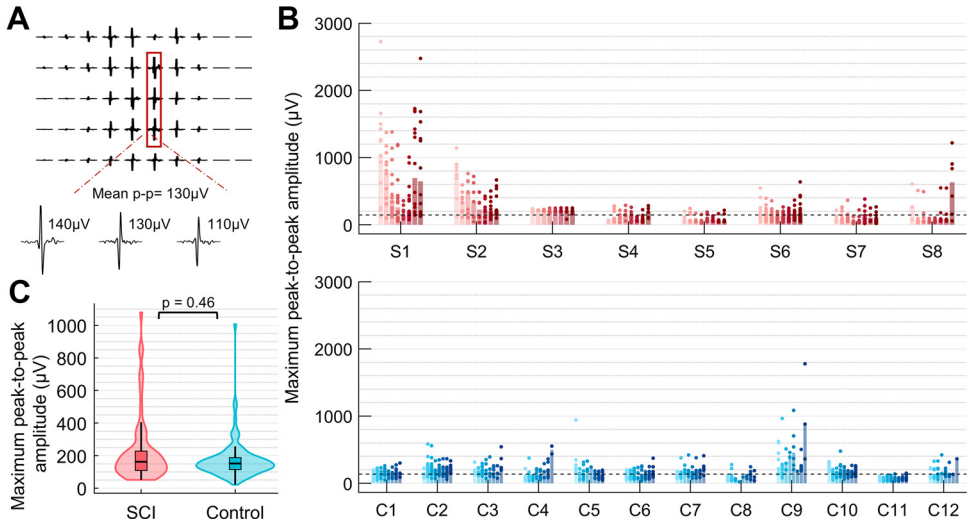

Figure 4. Motor unit maximum peak-to-peak amplitude. *A*: example of obtained motor unit action potential shapes after spike-triggered averaging. The three action potentials with higher amplitudes are highlighted (red rectangle), and their peak-to-peak values are shown, together with their mean value. *B*: peak-to-peak amplitude distributions across all participants and tasks for each group, spinal cord injury (SCI; red gradient) and control (blue gradient), with the median values as the black dashed line. The dots are the peak-to-peak amplitudes of each motor unit. The bars correspond to the median amplitude for each hand movement task and their color represents the tasks, in the following order, left to right: thumb, index, middle, ring, pinkie, two and three-finger pinches, and opening and closing of the fingers. *C*: distributions of peak-to-peak amplitudes averaged for each task and participant, SCI (pink) and control (blue), with violin plots normalized by area.

area distributions (Fig. 5*B*) were significantly different between groups, $P = 1.996\text{e-}06$, $t(1384) = 4.774$, $\beta = 0.0502$. At a participant-specific level, we observed that S4, S5, and S7 presented the largest areas in comparison with the other SCI and control participants (Fig. 5*C*).

Motor Unit Relative Depth

We decided to investigate the association between motor unit area and motor unit amplitude since this could provide information about the relative depth of the motor units in the volume conductor (Fig. 6*A*). We found a weak negative correlation between peak-to-peak amplitude and area values for the SCI group ($r = -0.084$, $P = 0.037$). Motor units with very high areas presented lower peak-to-peak amplitudes, whereas motor units with very high peak-to-peak amplitudes presented low area values. For the control group, we also observed a weak negative correlation ($r = -0.135$, $P = 1.736\text{e-}04$).

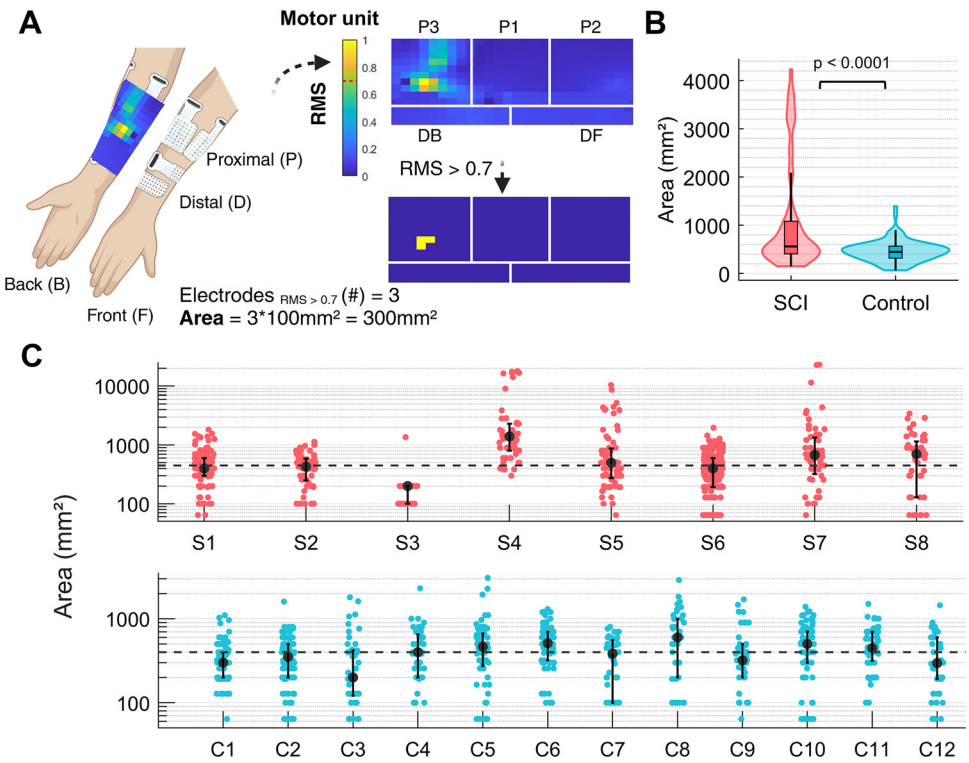

Figure 5. Motor unit area. *A*: after applying a spike-triggered average method, a spatial map of root-mean-square (RMS) values for each motor unit was obtained. The spatial map values were normalized between 0 and 1, according to the motor unit maximum and minimum RMS values. The area of activity was defined based on a threshold of 0.7 of normalized RMS values. This area was calculated based on the number of electrodes or pixels above the threshold and multiplied by the area of the corresponding electrode grid (100 mm^2 for an 8×8 grid and 64 mm^2 for a 13×5 grid). *B*: distribution of areas per group, averaged for each task and participant, spinal cord injury (SCI; pink) and control (blue), with violin plots normalized by area. *C*: distribution of motor unit areas across all participants and tasks for each group, SCI (red gradient) and control (blue gradient), with the median value for each group shown as the black dashed line. The dots represent the area of each motor unit. The plots are shown using a semi-log scale (*y* axis) for better visualization. *A*: image created with a licensed version of BioRender.org.

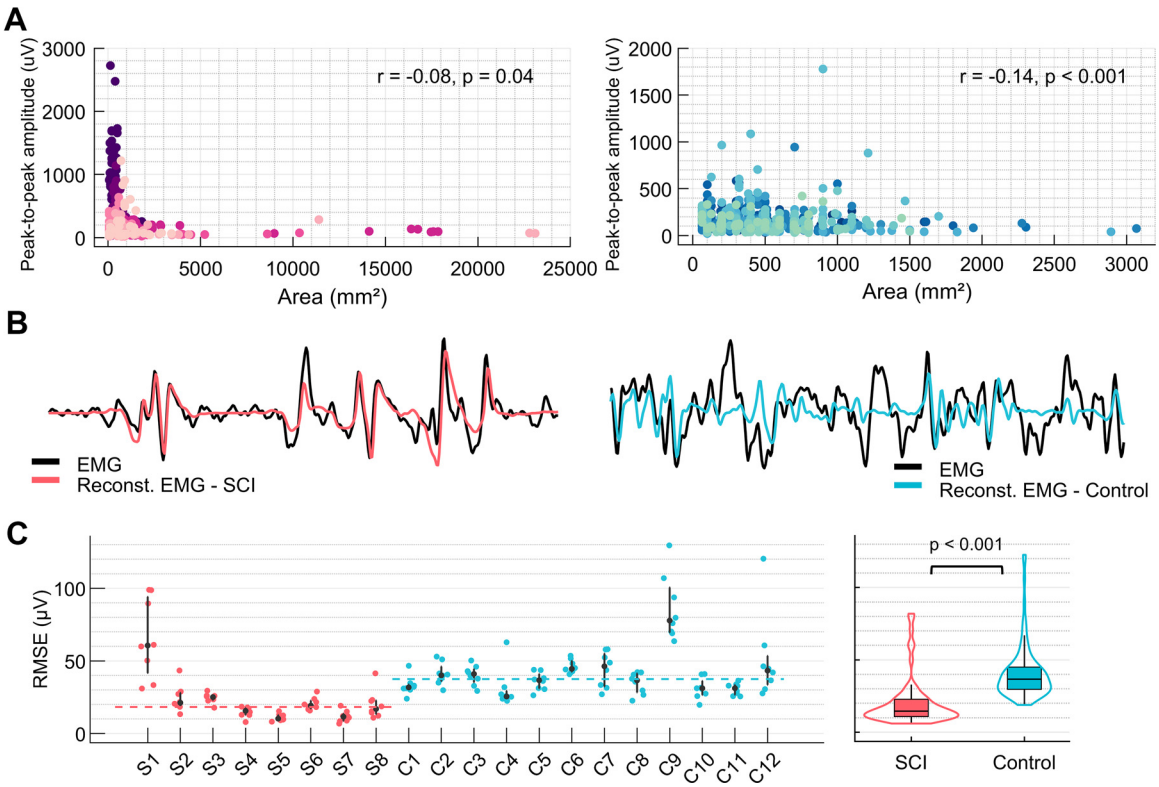

Figure 6. *A*: relationship between peak-to-peak amplitude (μV) and motor unit area per group, together with Spearman correlation values [spinal cord injury (SCI) in pink, control in blue]. Dots correspond to the individual motor units; the different colors represent the participants. Note that the plots are presented in different scales, SCI (*y* axis: 0–3,000 μV; *x* axis: 0–25,000 mm^2) and control (0–2,000 μV; 0–3,200 mm^2). *B*: example of original (in black) and reconstructed EMG signals for one electrode channel (SCI in pink, control in blue), 200-ms window. *C*, *left*: root mean square error (RMSE) between original and reconstructed EMG for each task across participants for both SCI and control groups. The dots represent the RMSE values for each task and the dashed line shows the median across groups (SCI in pink and control in blue). *Right*: box plot summarizing the distribution of RMSE for both groups.

Reconstructed EMG Signals

We also assessed the error (RMSE) values between the acquired and reconstructed EMG signals (Fig. 6, *B* and *C*). With this analysis, we aimed to determine whether a smaller number of undecomposed motor units (low error) in one group could explain the differences we observed in the area and peak-to-peak amplitude values. Overall, we observed lower RMSE values in SCI – 14.55 μV (10.80, 22.78) in comparison with the control group – 36.64 μV (29.64, 45.01), (P = 1.65e-5, β = −33.733, $t(144)$ = −4.458). These lower values demonstrate that we decomposed a higher proportion of motor units from HDsEMG signals from the SCI group.

DISCUSSION

In this study, we analyzed motor unit data from SCI and control groups, and we were able to decode the same motor unit modes corresponding to flexion and extension of individual fingers from participants in both groups, despite between-group differences in motor unit control. Interestingly, the SCI group had more nonmodulated motor units than the control group. This could be because of maladaptive changes due to inactivity after SCI, spasticity, and tonic motor unit firing (40, 41), and/or a reduction in their ability to voluntarily control motor units. It is difficult to rule out any of these possibilities as SCI participants spent years without attempting hand movements and were unable to move their fingers. Based on the subjective feedback of these participants during our experiments, they required considerable focus and effort to attempt the tasks.

Nonetheless, the latent factor analysis revealed that two modes explained most of the motor unit firings variance for the SCI group as well as the control group. These two modes represent common inputs to motor units. As common fluctuations in motor unit discharge activity represent inherent characteristics of voluntary motor control (42, 43), this demonstrates that after SCI, we can decode voluntary movement intent and common input from paralyzed muscles. When analyzing the cross-correlation values between the modes and reference kinematics, we found strong associations between these modes and flexion and extension movements. The differences between the cross-correlation values from SCI and control groups indicate a greater difficulty in maintaining patterned motor unit activity after SCI. However, the similar lag values between the groups suggest that motor units were properly recruited in response to the visual feedback from the virtual hand and that common input to motor neurons is preserved, even after SCI. This could mean that, as in stroke (44), residual neural pathways can recruit motor units, but the discharge rate modulation is impaired.

The high percentage of nonmodulated motor units for each participant with SCI provides evidence that there are motor units potentially not responding to modulatory

voluntary inputs. These motor units likely lowered the cross-correlation values between the flexion and extension motor unit modes and reference kinematics in the SCI group. Our results are in line with a previous study for the thenar muscles in chronic cervical SCI, in which regular and irregular firing motor units were observed (18). Future neural interfacing algorithms should consider removing nonmodulated motor unit activity to improve the performance of motor neuron-computer interfaces. These nonmodulated motor units are probably related to involuntary muscle contractions present in SCI and other maladaptive changes after the injury. Only S6 and S8 presented a higher number of modulated motor units compared with the other SCI participants. When analyzing the characteristics of each participant, we found that S6 and S8 had the shortest time since injury, reduced spasticity, and the lowest level with normal sensory function at T1 and T3, respectively. The main reason for the improved voluntary motor unit control is still unclear, as other participants have at least one of the above characteristics, for example, S1 and S7. We speculate that this might be due to an intact sensory pathway at the C5/C6 injury level, and some degree of spasticity, which has been reported to indicate residual descending connectivity (45).

It is important to note that motor units with a high variance of phase difference, classified as nonmodulated, may still be active during both the flexor and extensor phases of the movement. Although these motor units exhibit some degree of modulation, their activity does not appear to be directly associated with task execution. We believe that these motor units are related to unintentional movement of fingers not directly involved in the task or encoding tonic/spastic potentials. This tonic activity may be encoding the posture of the wrist, as similar patterns were observed in the control group [see Oßwald et al. (46) for more details]. Future studies that directly examine this are needed.

When comparing the motor unit classification based on the weight coefficients from the NNMF results and phase difference variance, we observed that more motor units are classified as nonmodulated in the SCI group for both analyses. However, the NNMF-based classification relies on the quality of the motor unit modes extracted, corresponding to an approximation of the motor unit data set. In contrast, the variance of phase difference provides a direct analysis of the motor unit firing patterns compared to the reference kinematics, with the defined threshold representing a more conservative approach.

The ultrasound recordings of the forearm extensor muscles during the instructed hand movements showed local displacements within these muscles after SCI, even though no actual hand movement was observed. The tissue displacement was muscle region-specific and was dependent on the attempted task and the spatial location of the decomposed motor units. The moderate cross-correlation between the magnitudes of the velocities computed from the ultrasound recordings and the smoothed motor unit spike trains provides additional evidence that the forearm extensor muscles were being voluntarily controlled. We also found clear differences in muscle activities between movements that could actually be voluntarily performed by the participant (wrist flexion and extension) and another task that involved no movement because it was performed by the paralyzed digits. Further evidence of the association between muscle movement and EMG activity is provided by the observed delays between neural activity recorded by HDsEMG and tissue displacement recorded by ultrasound, which are comparable to those described in the literature in abled-body participants (30). Overall, the muscle ultrasound was able to detect complementary aspects related to motor unit activation.

We investigated several other aspects related to motor unit activation, including motor unit action potential amplitude. Previous literature suggests that high amplitudes might indicate reinnervation by collateral sprouting after SCI, although this is not observed in all individuals (7, 16). In our study, most of the SCI group participants presented motor unit peak-to-peak amplitudes in the same range as those from the control group, consistent with the findings of Yang et al. (7). We found abnormal peak-to-peak amplitudes in only one participant from the SCI group (S1).

To better understand the spatial territory of motor unit activity, we computed the area of individual motor units. We found an enlarged area for the SCI group, which could be due to sprouting and other anatomical changes after injury (6). Since the area represents the surface within the forearm muscle in which the muscle fibers of individual motor units could be distributed, a more dispersed activity of an individual motor unit could mean that muscle fiber reinnervation occurred by motor neuron axons in different areas of the muscles. However, it is important to note the very high motor unit areas from the SCI group could also be caused by crosstalk from neighboring muscles. Different area values between the groups might also be the result of muscle atrophy and corresponding muscle architectural and geometrical changes (47–49). Future studies involving high-density intramuscular recordings are needed to help characterize the geometrical relations between neural and spatial properties of the motor units.

We also examined the relative depth of the active motor units, which is related to the motor unit action potential amplitude and area, and we found a weak negative correlation between motor unit amplitude and area in both the SCI and control groups. We found motor units with a very large area and low amplitude, which we consider as deep motor units, as well as motor units with a small area and high amplitude, which we consider as superficial motor units. Based on these assumptions, we speculate that the motor units we detected from SCI participants were relatively deep in comparison to those from the control participants, despite evidence that EMG is biased towards large and superficial motor units (50, 51). We believe that relatively deeper motor units were detected from SCI participants because they have fewer functional motor units left after the injury. Therefore, these participants voluntarily recruit fewer motor units, which facilitates the detection of these motor units by decomposition algorithms.

To investigate whether this detection of relatively deeper motor units is related to the recruitment of fewer motor units in SCI, we analyzed the RMSE values between the original and reconstructed EMG, which indicate the amount of undecomposed motor units. In the SCI group, we observed lower RMSE values compared with the control group, suggesting that the EMG signals from SCI

participants were reconstructed more accurately based on the decomposed motor unit spike trains. The only exception was participant S1, who showed motor units with very high peak-to-peak amplitudes. We then considered the correlation between the RMSE values and both amplitude and area of the motor units but did not find a significant association. These results should be interpreted with caution, as they do not imply we detected more deep (or less superficial) motor units from SCI participants.

The absence of many active motor units from participants with SCI and possibly different anatomical characteristics might have allowed us to detect a larger range of motor units with different properties from the HDsEMG signals in this group. Nevertheless, our analysis of EMG reconstruction strongly suggests that the EMG signals from the SCI group reflect less motor unit recruitment. The firings from these recruited motor units can be decomposed with high accuracy because a lower number of recruited motor units increases the quality of the decomposition (33). The decomposition is further facilitated by the fact that participants with SCI were only attempting the hand movements with no force or not enough force to move the fingers, as they were unable to do so due to the injury. In contrast, the control group performed dynamic movements, which are known to present challenges for decomposition due to muscle shortening upon activation and muscle length changes during movement (52). This finding might explain the similar number of motor units detected in the SCI and control groups, given that identifying most of the active motor units for the control group is more challenging.

A few limitations might have influenced our results. These were the limited number of SCI participants, and the relatively short-duration familiarization period (20–30 s). The results from this study were obtained after one main laboratory visit, only with one type of task (flexion and extension of the digits at 0.5 Hz), and without any real-time and closed-loop training. Using motor unit feedback training in a closed loop with the participant and incorporating different tasks might improve these results (53). In addition, including data from other stages of the injury, such as subacute SCI, could provide further insights into motor unit changes after SCI. Our main limitations are due to the reduced number of motor units identified from HDsEMG, which is restricted to recording electrical activity from superficial regions of the muscles, as well as the physiological differences among the participants i.e., volume conductor differences. Hence, our estimation of spatial properties might be influenced by muscle size, fat infiltration, subcutaneous fat tissue, and other tissues interposed between the electrodes and muscles beneath the electrodes (51, 54). In conclusion, even though we found differences in the number of modulated motor units between the SCI and control groups, we could still decode the same two motor unit modes, which appear to encode flexion and extension of the fingers. This clarifies that muscle activity can be used for real-time decoding of movement intention after SCI in paralyzed muscles, as we have previously shown (22). In addition, the number of nonmodulated motor units, either tonically or irregularly firing, must be considered when developing control algorithms. Overall, we observed that SCIs are very diverse among individuals, even at the same level of injury, and that this is reflected by variable motor unit behavior and properties that can be assessed after SCI with HDsEMG noninvasively. Characterizing motor unit behavior and property changes after SCI is essential to obtain a proper assessment of injury severity and the natural recovery phase, and could aid in providing adequate therapy and treatments by taking plasticity and residual activity into account.

DATA AVAILABILITY

Source data for this study are not publicly available due to privacy or ethical restrictions. The source data are available to verified researchers upon request by contacting the corresponding author.

SUPPLEMENTAL MATERIAL

Supplemental Figs. S1–S3 and Supplemental Table S1: https://doi.org/10.6084/m9.figshare.27992570; Supplemental Video S1: https://doi.org/10.6084/m9.figshare.27992768.

ACKNOWLEDGMENTS

We thank all the participants who contributed to this work and Marius Oßwald for the decomposition of the control group data. Figures were created using the Gramm toolbox (55), and Biorender was used to create the schematic in Fig. 5*A*.

GRANTS

This work was partially supported by the d.hip campus-bavarian aim, a cooperation between Siemens Healthineers, Medical Valley, University Hospital Erlangen, and Friedrich-Alexander University (to A.D.V. and D.S.O.); the European Research Council (ERC) Starting Grant project GRASPAGAIN under grant 101118089 (to A.D.V.); the German Ministry for Education and Research (BMBF) through the project MYOREHAB under Grant 01DN2300 (to A.D.V.).

DISCLOSURES

No conflicts of interest, financial or otherwise, are declared by the authors.

AUTHOR CONTRIBUTIONS

D.S.O., M.C., B.J.R., A.B., M.P., and A.D.V. conceived and designed research; D.S.O., B.J.R., and A.B. performed experiments; D.S.O., M.C., B.J.R., and A.B. analyzed data; D.S.O., M.C., B.J.R., A.B., and A.D.V. interpreted results of experiments; D.S.O. and M.C. prepared figures; D.S.O. and M.C. drafted manuscript; D.S.O., M.C., B.J.R., A.B., M.P., and A.D.V. edited and revised manuscript; D.S.O., M.C., B.J.R., A.B., M.P., and A.D.V. approved final version of manuscript.

REFERENCES

1. **Oudega M**, **Perez MA.** Corticospinal reorganization after spinal cord injury. *J Physiol* 590: 3647–3663, 2012. doi:10.1113/jphysiol.2012.233189.
2. **Grumbles RM**, **Thomas CK.** Motoneuron death after human spinal cord injury. *J Neurotrauma* 34: 581–590, 2017. doi:10.1089/neu.2015.4374.
3. **Dietz V**, **Müller R.** Degradation of neuronal function following a spinal cord injury: Mechanics and countermeasures. *Brain* 127: 2221–2231, 2004. doi:10.1093/brain/awh255.
4. **Gorassini MA**, **Knash ME**, **Harvey PJ**, **Bennett DJ**, **Yang JF.** Role of motoneurons in the generation of muscle spasms after spinal cord injury. *Brain* 127: 2247–2258, 2004. doi:10.1093/brain/awh243.

5. **Thomas CK**, **Bakels R**, **Klein CS**, **Zijdewind I.** Human spinal cord injury: Motor unit properties and behaviour. *Acta Physiol (Oxf)* 210: 5–19, 2014. doi:10.1111/apha.12153.
6. **Anderson MA**, **Squair JW**, **Gautier M**, **Hutson TH**, **Kathe C**, **Barraud Q**, **Bloch J**, **Courtine G.** Natural and targeted circuit reorganization after spinal cord injury. *Nat Neurosci* 25: 1584–1596, 2022. doi:10.1038/s41593-022-01196-1.
7. **Yang JF**, **Stein RB**, **Jhamandas J**, **Gordon T.** Motor unit numbers and contractile properties after spinal cord injury. *Ann Neurol* 28: 496–502, 1990. doi:10.1002/ana.410280405.
8. **Raineteau O**, **Schwab ME.** Plasticity of motor systems after incomplete spinal cord injury. *Nat Rev Neurosci* 2: 263–273, 2001. doi:10.1038/35067570.
9. **Tan AM**, **Chakrabarty S**, **Kimura H**, **Martin JH.** Selective corticospinal tract injury in the rat induces primary afferent fiber sprouting in the spinal cord and hyperreflexia. *J Neurosci* 32: 12896–12908, 2012. doi:10.1523/JNEUROSCI.6451-11.2012.
10. **Courtine G**, **Sofroniew MV.** Spinal cord repair: advances in biology and technology. *Nat Med* 25: 898–908, 2019., doi:10.1038/s41591-019-0475-6.
11. **Kirshblum S**, **Snider B**, **Eren F**, **Guest J.** Characterizing natural recovery after traumatic spinal cord injury. *J Neurotrauma* 38: 1267–1284, 2021. doi:10.1089/neu.2020.7473.
12. **Rodrigues LF**, **Moura-Neto V**, **E Spohr TCLS.** Biomarkers in spinal cord injury: from prognosis to treatment. *Mol Neurobiol* 55: 6436–6448, 2018. doi:10.1007/s12035-017-0858-y.
13. **Kramer JLK**, **Geisler F**, **Ramer L**, **Plunet W**, **Cragg JJ.** Open access platforms in spinal cord injury: existing clinical trial data to predict and improve outcomes. *Neurorehabil Neural Repair* 31: 399–401, 2017. doi:10.1177/1545968316688801.
14. **Thomas CK**, **Häger CK**, **Klein CS.** Increases in human motoneuron excitability after cervical spinal cord injury depend on the level of injury. *J Neurophysiol* 117: 684–691, 2017. doi:10.1152/jn.00676.2016.
15. **Takeoka A**, **Vollenweider I**, **Courtine G**, **Arber S.** Muscle spindle feedback directs locomotor recovery and circuit reorganization after spinal cord injury. *Cell* 159: 1626–1639, 2014. doi:10.1016/j.cell.2014.11.019.
16. **Franz S**, **Eck U**, **Schuld C**, **Heutehaus L**, **Wolf M**, **Wilder-Smith E**, **Schulte-Mattler W**, **Weber M-A**, **Rupp R**, **Weidner N.** Lower motoneuron dysfunction impacts spontaneous motor recovery in acute cervical spinal cord injury. *J Neurotrauma* 40: 862–875, 2023. doi:10.1089/neu.2022.0181.
17. **Zakrasek EC**, **Jaramillo JP**, **Lateva ZC**, **Punj V**, **Kiratli BJ**, **McGill KC.** Quantitative electrodiagnostic patterns of damage and recovery after spinal cord injury: a pilot study. *Spinal Cord Ser Cases* 5: 101, 2019., doi:10.1038/s41394-019-0246-0.
18. **Zijdewind I**, **Thomas CK.** Firing patterns of spontaneously active motor units in spinal cord-injured subjects. *J Physiol* 590: 1683–1697, 2012. doi:10.1113/jphysiol.2011.220103.
19. **Thomas CK**, **Broton JG**, **Calancie B.** Motor unit forces and recruitment patterns after cervical spinal cord injury. *Muscle Nerve* 20: 212–220, 1997. doi:10.1002/(SICI)1097-4598(199702)20:2<212::AID-MUS12>3.0.CO;2-4.
20. **Ting JE**, **Del Vecchio A**, **Sarma D**, **Verma N**, **Colachis SC**, **Annetta NV**, **Collinger JL**, **Farina D**, **Weber DJ.** Sensing and decoding the neural drive to paralyzed muscles during attempted movements of a person with tetraplegia using a sleeve array. *J Neurophysiol* 126: 2104–2118, 2021. doi:10.1152/jn.00220.2021.
21. **Sharma P**, **Naglah A**, **Aslan S**, **Khalifa F**, **El-Baz A**, **Harkema S**, **D'Amico J.** Preservation of functional descending input to paralyzed upper extremity muscles in motor complete cervical spinal cord injury. *Clin Neurophysiol* 150: 56–68, 2023. doi:10.1016/j.clinph.2023.03.003.
22. **Oliveira DS**, **Ponfick M**, **Braun DI**, **Osswald M**, **Sierotowicz M**, **Chatterjee S**, **Weber D**, **Eskofier B**, **Castellini C**, **Farina D**, **Kinfe TM**, **Del Vecchio A.** A direct spinal cord–computer interface enables the control of the paralysed hand in spinal cord injury. *Brain* 147: 3583–3595, 2024. doi:10.1093/brain/awae088.
23. **McKay WB**, **Lim HK**, **Priebe MM**, **Stokic DS**, **Sherwood AM.** Clinical neurophysiological assessment of residual motor control in post-spinal cord injury paralysis. *Neurorehabil Neural Repair* 18: 144–153, 2004. doi:10.1177/0888439004267674.
24. **Sherwood AM**, **Dimitrijevic MR**, **McKay WB.** Evidence of subclinical brain influence in clinically complete spinal cord injury: discomplete SCI. *J Neurol Sci* 110: 90–98, 1992. doi:10.1016/0022-510X(92)90014-C.
25. **Sherwood AM**, **Priebe MM**, **Graves DE.** Consistency of multi-channel surface EMG recordings: application in spinal cord injured subjects. *J Electromyogr Kinesiol* 7: 97–111, 1997. doi:10.1016/S1050-6411(96)00027-2.
26. **Dimitrijevic MR**, **Dimitrijevic MM**, **Faganel J**, **Sherwood AM.** Suprasegmentally induced motor unit activity in paralyzed muscles of patients with established spinal cord injury. *Ann Neurol* 16: 216–221, 1984. doi:10.1002/ana.410160208.
27. **Cakici AL**, **Osswald M**, **De Oliveira DS**, **Braun DI**, **Simpetru RC**, **Kinfe T**, **Eskofier BM**, **Del Vecchio A.** A generalized framework for the study of spinal motor neurons controlling the human hand during dynamic movements. *Annu Int Conf IEEE Eng Med Biol Soc* 2022: 4115–4118, 2022. doi:10.1109/EMBC48229.2022.9870914.
28. **Botter A**, **Vieira TMM**, **Loram ID**, **Merletti R**, **Hodson-Tole EF.** A novel system of electrodes transparent to ultrasound for simultaneous detection of myoelectric activity and B-mode ultrasound images of skeletal muscles. *J Appl Physiol (1985)* 115: 1203–1214, 2013. doi:10.1152/japplphysiol.00090.2013.
29. **Carbonaro M**, **Meiburger KM**, **Seoni S**, **Hodson-Tole EF**, **Vieira T**, **Botter A.** Physical and electrophysiological motor unit characteristics are revealed with simultaneous high-density electromyography and ultrafast ultrasound imaging. *Sci Rep* 12: 8855, 2022. doi:10.1038/s41598-022-12999-4.
30. **Martinez-Valdes E**, **Negro F**, **Botter A**, **Pincheira PA**, **Cerone GL**, **Falla D**, **Lichtwark GA**, **Cresswell AG.** Modulations in motor unit discharge are related to changes in fascicle length during isometric contractions. *J Appl Physiol (1985)* 133: 1136–1148, 2022. doi:10.1152/japplphysiol.00758.2021.
31. **Cerone GL**, **Botter A**, **Gazzoni M.** A modular, smart, and wearable system for high density sEMG detection. *IEEE Trans Biomed Eng* 66: 3371–3380, 2019. doi:10.1109/TBME.2019.2904398.
32. **Holobar A**, **Zazula D.** Multichannel blind source separation using convolution Kernel compensation. *IEEE Trans Signal Process* 55: 4487–4496, 2007. doi:10.1109/TSP.2007.896108.
33. **Del Vecchio A**, **Holobar A**, **Falla D**, **Felici F**, **Enoka RM**, **Farina D.** Tutorial: analysis of motor unit discharge characteristics from high-density surface EMG signals. *J Electromyogr Kinesiol* 53: 102426, 2020. doi:10.1016/j.jelekin.2020.102426.
34. **Del Vecchio A**, **Marconi Germer C**, **Kinfe TM**, **Nuccio S**, **Hug F**, **Eskofier B**, **Farina D**, **Enoka RM.** The forces generated by agonist muscles during isometric contractions arise from motor unit synergies. *J Neurosci* 43: 2860–2873, 2023. doi:10.1523/JNEUROSCI.1265-22.2023.
35. **Weinman LE**, **Del Vecchio A**, **Mazzo MR**, **Enoka RM.** Motor unit modes in the calf muscles during a submaximal isometric contraction are changed by brief stretches. *J Physiol* 602: 1385–1404, 2024. doi:10.1113/JP285437.
36. **Lee DD**, **Seung HS.** Learning the parts of objects by non-negative matrix factorization. *Nature* 401: 788–791, 1999. doi:10.1038/44565.
37. **Berens P.** Circular Statistics Toolbox (Directional Statistics) (Online). MATLAB Help Center, 2024. https://www.mathworks.com/matlabcentral/fileexchange/10676-circular-statistics-toolbox-directional-statistics [2024 Dec 4].
38. **Barron JL**, **Fleet DJ**, **Beauchemin SS.** Performance of optical flow techniques. *Int J Comput Vision* 12: 43–77, 1994. doi:10.1007/BF01420984.
39. **Del Vecchio A**, **Negro F**, **Felici F**, **Farina D.** Associations between motor unit action potential parameters and surface EMG features. *J Appl Physiol (1985)* 123: 835–843, 2017. doi:10.1152/japplphysiol.00482.2017.
40. **Fong AJ**, **Roy RR**, **Ichiyama RM**, **Lavrov I**, **Courtine G**, **Gerasimenko Y**, **Tai YC**, **Burdick J**, **Edgerton VR.** Recovery of control of posture and locomotion after a spinal cord injury: solutions staring us in the face. *Prog Brain Res* 175: 393–418, 2009. doi:10.1016/S0079-6123(09)17526-X.
41. **Mahrous A**, **Birch D**, **Heckman C**, **Tysseling V.** Muscle spasms after spinal cord injury stem from changes in motoneuron excitability and synaptic inhibition, not synaptic excitation. *J Neurosci* 44: e1695232023, 2024. doi:10.1523/jneurosci.1695-23.2023.
42. **Farina D**, **Negro F**, **Dideriksen JL.** The effective neural drive to muscles is the common synaptic input to motor neurons. *J Physiol* 592: 3427–3441, 2014. doi:10.1113/jphysiol.2014.273581.

43. **Negro F**, **Yavuz UŞ**, **Farina D.** The human motor neuron pools receive a dominant slow-varying common synaptic input. *J Physiol* 594: 5491–5505, 2016. doi:10.1113/JP271748.
44. **Mottram CJ**, **Heckman CJ**, **Powers RK**, **Rymer WZ**, **Suresh NL.** Disturbances of motor unit rate modulation are prevalent in muscles of spastic-paretic stroke survivors. *J Neurophysiol* 111: 2017–2028, 2014. doi:10.1152/jn.00389.2013.
45. **Sangari S**, **Chen B**, **Grover F**, **Salsabili H**, **Sheth M**, **Gohil K**, **Hobbs S**, **Olson A**, **Eisner-Janowicz I**, **Anschel A**, **Kim K**, **Chen D**, **Kessler A**, **Heinemann AW**, **Oudega M**, **Kwon BK**, **Kirshblum S**, **Guest JD**, **Perez MA.** Spasticity predicts motor recovery for patients with subacute motor complete spinal cord injury. *Ann Neurol* 95: 71–86, 2024. doi:10.1002/ana.26772.
46. **Oßwald M**, **Cakici AL**, **de Oliveira DS**, **Braun DI**, **Vecchio AD.** Mechanical hand synergies during dynamic hand movements are mostly controlled in a non-synergistic way by spinal motor neurons (Preprint). *bioRxiv*, 2023. doi:10.1101/2023.07.25.550369.
47. **Vieira TM**, **Botter A.** The accurate assessment of muscle excitation requires the detection of multiple surface electromyograms. *Exerc Sport Sci Rev* 49: 23–34, 2021. doi:10.1249/JES.0000000000000240.
48. **Gorgey AS**, **Dudley GA.** Skeletal muscle atrophy and increased intramuscular fat after incomplete spinal cord injury. *Spinal Cord* 45: 304–309, 2007. doi:10.1038/sj.sc.3101968.
49. **Castro MJ**, **Apple DF**, **Hillegass EA**, **Dudley GA.** Influence of complete spinal cord injury on skeletal muscle cross-sectional area within the first 6 months of injury. *Eur J Appl Physiol Occup Physiol* 80: 373–378, 1999. doi:10.1007/s004210050606.
50. **Farina D**, **Holobar A**, **Merletti R**, **Enoka RM.** Decoding the neural drive to muscles from the surface electromyogram. *Clin Neurophysiol* 121: 1616–1623, 2010. doi:10.1016/j.clinph.2009.10.040.
51. **Besomi M**, **Hodges PW**, **Van Dieën J**, **Carson RG**, **Clancy EA**, **Disselhorst-Klug C**, **Holobar A**, **Hug F**, **Kiernan MC**, **Lowery M**, **McGill K**, **Merletti R**, **Perreault E**, **Søgaard K**, **Tucker K**, **Besier T**, **Enoka R**, **Falla D**, **Farina D**, **Gandevia S**, **Rothwell JC**, **Vicenzino B**, **Wrigley T.** Consensus for experimental design in electromyography (CEDE) project: electrode selection matrix. *J Electromyogr Kinesiol* 48: 128–144, 2019. doi:10.1016/j.jelekin.2019.07.008.
52. **Glaser V**, **Holobar A.** Motor unit identification from high-density surface electromyograms in repeated dynamic muscle contractions. *IEEE Trans Neural Syst Rehabil Eng* 27: 66–75, 2019. doi:10.1109/TNSRE.2018.2885283.
53. **Braun DI**, **De Oliveira DS**, **Bayer P**, **Ponfick M**, **Mehari Kinfe T**, **Del Vecchio A.** NeurOne: high-performance motor unit-computer interface for the paralyzed (Preprint). *medRxiv*, 2023. doi:10.1101/2023.09.25.23295902.
54. **Oliveira D. S D**, **Casolo A**, **Balshaw TG**, **Maeo S**, **Lanza MB**, **Martin NRW**, **Maffulli N**, **Kinfe TM**, **Eskofier BM**, **Folland JP**, **Farina D**, **Del Vecchio A.** Neural decoding from surface high-density EMG signals: influence of anatomy and synchronization on the number of identified motor units. *J Neural Eng* 19: 046029, 2022. doi:10.1088/1741-2552/ac823d.
55. **Morel P.** Gramm: grammar of graphics plotting in Matlab. *JOSS* 3: 568, 2018. doi:10.21105/joss.00568.